# Depth distribution profile of martensite phase observed by transmission electron microscope in ion implanted metals

Dwi Gustiono [1,2*]

[1]*Ibnu Sina Institute for Fundamental Science Studies, UTM, 81310 UTM Skudai, Johor, Malaysia*
[2]*Badan Pengkajian dan Penerapan Teknologi, Jalan. MH THamrin 8 - Jakarta 10340, Indonesia*

## ABSTRACT

In this work, transmission electron microscopy (TEM) observation results from a depth distribution profile of the nano-martensite occuring in titanium implanted austenitic stainless steel is presented. The thickness of 200 keV high-energy ion implantation induced layer until 150 nm as calculated by the TRIM computer simulation based on the Monte-Carlo program. After the implantation, the specimens were attached to thin foil ring to be milled by focused ion beam (FIB). TEM observation on the ion implantation induced layer reveled that nano-martensite is distributed until80 nm under surface. the nano-martensite mostly nucleated at the region near the surface occurred the higher concentration gradient of implanted ion, namely higher stress concentration takes place so that this stress introduced due to the implanted ions act as a driving force for the transformation.

| Transmission electron microscope | Ion Implantation|  Metals | Depth distribution profile | Martensite |

## 1. INTRODUCTION

Martensitic phase transformation from $\gamma$ (fcc) to $\alpha$ (bcc) in austenitic stainless steels can be induced by ion implantations [1-8]. An investigation was carried out using conversion electron Mossbauer spectroscopy (CEMS) in 17/7 stainless steel implanted with inert gas (Kr, Ar) ions and the stainless steel constituent element (Fe, Ni, Cr) ions established that the primary contribution to the driving force for these transformations comes from relief of high stress levels in the implanted layer [3]. The highest efficiency of the transformation was observed after implantation with inert-gas ions, known to form highly pressurized inclusions containing the heavier inert gases in the solid phase at room temperature [3,9]. On the other hand, implantations with the $\alpha$ stabilizing stainless steel constituent elements (Fe and Cr) will only lead to martensitic transformations when the implant concentrations about 10-15 at.%, where is the phase stability of the implanted layer is totally altered [3,10]. An analysis was done by in-situ Rutherford backscattering (RBS)/channeling analysis, X-ray diffraction, and cross-section transmission electron microscopy (XTEM) to the austenitic stainless steel implanted 230 keV $Xe^+$ ions found that the martensitic transformation is induced by high level of stress originated from the presence of dense distributions of solid crystalline Xe inclusions on top of a much thicker

layer where is the pressure in the inclusions is determined about 5 GPa [11]. It has been established that the martensitic transformation nucleates at the surface and is gradually driven to larger depth with increasing ion fluence [12]. However, the driving force responsible for these martensitic transformation remain uncertain.

In the present study would be revealed that in the case of ion implantation by stabilizer ion ($Ti^+$), the concentration gradient of the implanted ions plays more important rule for the driving force of the martensitic transformation.

## 2. EXPERIMENTAL

Cross-sectional specimens were made from the SUS-304 stainless steels plate sized 2 x 0.5 x $0.07$ $mm^3$ and had been mechanically polished and annealed at 1323 K in vacuum for 30 minutes, and then directly quenched in water. After that the specimens were implanted by $Ti^+$ ion. After the implantation, the specimens were attached to thin foil ring to be milled by FIB. Before milling process by 30 keV $Ga^+$ ions, each of implanted surfaces to be milled was coated by W layer to protect the surface damage during milling with 30 keV $Ga^+$ ions by FIB. In this procedure, each of specimen to be milled need four steps milling processes, namely the first and the second ones are milling processes by ion beam to prepare the specimen with 40 and 20 μm in thickness, the third ones is milling by electron

*Corresponding author at Ibnu Sina Institute for Fundamental Science Studies,
Universiti Teknologi Malaysia, 81310 UTM Skudai, Johor, Malaysia.
E-mail addresses: gustiono@ibnusina.utm.my (Dwi Gustono Riban)*

beam to get specimen with1μm in thickness and the fourth step is polishing by electron to 0.1μm in thickness.

The ion implantation was carried out to dose of $5 \times 10^{20}$ Ti$^+$ ions m$^{-2}$ at 200 keV in room temperature using an ion accelerator. The possible local temperature increased due to highenergy ion irradiation was suggested less than about 50 K. The implanted ion range and vacancies range distributed during 200 keV in stainless steels calculated with TRIM code from the surface, as shown in the Figures 1. Calculation of the range distribution of the ion penetration has been made with the formalism of Monte-Carlo computer program by Biersack and Haggmark [3] in 1980. It has been developed for determining ion range and damage distributions as well as angular and energy distributions of backscattered and transmitted ions. The computer program provides particularly high computer efficiency and is also used to calculate the range distributions of a variety of ion/target combinations shown high precise with the experimental profiles.

Clarification to the calculation of the range distribution estimated with the Monte-Carlo computer program is carried out by the chemical compositions measurement by an energy dispersive X-ray (EDX) for the implanted regions, which is equipped with a TEM.

The best condition of a specimen would be observed by TEM corresponding to thickness less than 150 nm. Therefore, distribution range of the implanted ions was expected less than 150 nm. Thus theoretically calculation of the range distribution by TRIM code was important to be done. The calculation of the range distributions has been carried out by TRIM code based on the Monte-Carlo computer program and the calculation results is shown in the Figure 1.

The TEM investigations were performed by JEOL 2000FX and JEOL JEM-2010F TEM operated at 200 kV

## 3.     RESULTS & DISCUSSIO

Figure 2 shows a bright field image and corresponded SAD pattern of an un-implanted cross-sectional specimen. Figure 2(a) shows a microstructure of an interface between matrix (bright region) and tunsten (W) layer (dark region). Matrix region near the surface has some defects induced ion bombardment during W coating and milling use FIB. However, according to the SAD pattern in figure 2(b), the specimen had γ phase and was not found yet a phase transformation.
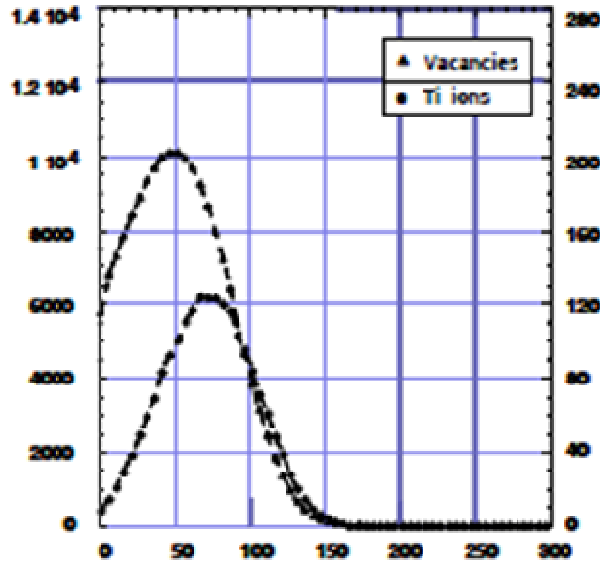


**Figure 1:** Depth distribution profile of ions and vacancies after implantation of 200 keV Ti ions to dose of $5 \times 10^{20}$ ions/m$^{-2}$ onto austenitic stainless steel are calculated using TRIM code computer program
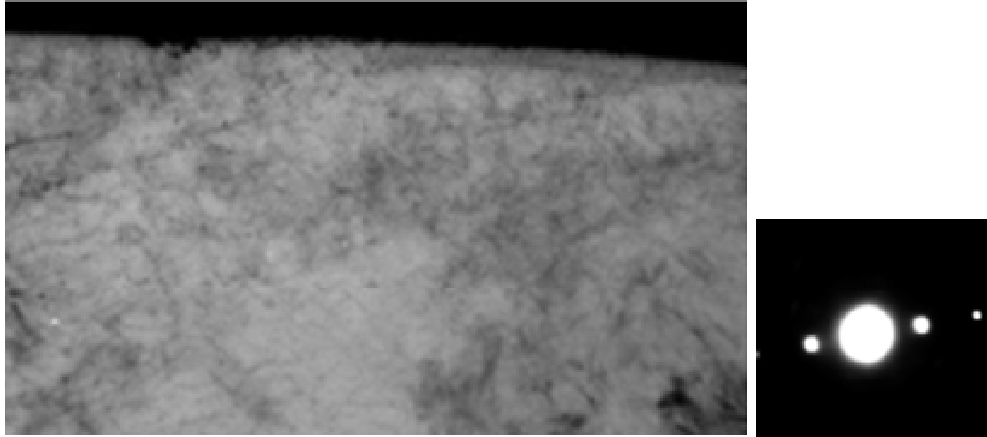
**Figure 2:** (a) TEM bright field image of onto austenitic stainless steel 301SS before implantation and (b) SAD patterns corresponded to the matrix

Figure 3 shows a bright field image of TEM and corresponding SAD patterns for cross-sectional of the specimens implanted with 200 keV $Ti^+$ ions to dose of $5x10^{20}$ ions $m^{-2}$ at room temperature. The dark contrast along outer surface is W coating layer which coated for the protection from the damage during FIB fabrication. After titanium ion implantation has high energy, according to TRIM calculation, some vacancies were created in the range about 150 nm under near the surface and the vacancies is concentrated at 50 nm under near the surface. On the other hand, titanium ions insert onto the matrix until 150 nm under near the surface and they were concentrated at 75 nm under near the surface. The dark contrast near surface indicated by arrow and suffixed to α is parts of matrix has phase transformed from face centered cubic (fcc/γ matrix) phase to base centered cubic (bcc/α) phase according to their SAD patterns as seen in the figure 3(b). This transformation is called with martensitic phase transformation. The martensite phase has variation in size, from 10 nm until 200 nm as seen in TEM observation to the plane specimen after implantation at same dose [13].

Figure 4 shows depth distribution profiles related with ion and vacancie ranges produced by $Ti^+$ implantation at 300 keV, were calculated by TRIM code and measured by EDX. The depth distribution profiles of $Ti^+$ ion calculated by TRIM code close to measured by EDX. All of the nano-martensite were induced in the range has high concentration gradient of ions and vacancies. EDX analysis results show that the $Ti^+$ ion concentration in the implanted regions less of 5 wt%. Figure 5 shows a bright field image of TEM for cross-sectional of the specimens implanted with 300 keV $Ti^+$ ions to dose of $5x10^{20}$ ions $m^{-2}$ at room temperature. The location of the nano-martensite nucleated is not coincident with the peaks of the implanted $Ti^+$ concentration, and the vacancies. This fact might suggest that the martensite phase transformation is not directly related to the implanted $Ti^+$ concentration. The phase transformation seem to be started at surface region away from the peak position of highest $Ti^+$ concentration, that is larger $Ti^+$ concentration difference (larger concentration gradient) which may gives rise the local stress concentration caused by lattice strain due to embedded $Ti^+$. The largest stress difference estimated from stress distribution calculated from $Ti^+$ concentration in stainless steel was caused at about 30-40 nm in depth. Furthermore the increasing the internal stress introduced by damage due to implantation may help the transformation. It is difficult to make estimation about the main stress as a driving force induced this transformation. However, the present results suggested that the stress contributed from the regions of larger concentration gradient play important rule for the transformation as revealed in the case of $Ti^+$ ion implantations.

There are three main effects [4,5,11] are suggested have possibility to contribute as a driving force responsible to the martensitic transformation induced by ion implantation. The first is primary radiation damages and point defects, the second is secondary damage effects such as precipitation or dispersion of the implanted ions, and the third is implantation-induced chemical compositional changes and alloying effects. The present and the previous investigation results were done by Johnson et al [1,2,3,11,12] and Hayashi et al [4,5,10,13] using TEM, GXRD, RBS and DCEMS revealed that the third effect is not significant in the case of inert gas ion implantations because implantation of inert gas ion is more efficient in inducing the transformation than constituent elements ion and stabilizer ion implantations. Ion implantation by constituent element ions and stabilizer ions functioned to stabilization of the martensitic phase induced the stress in accordance with the Schaeffler's diagram. Their experimental results to austenitic stainless steels implanted by both light($H^+$, $He^+$, $D^+$) and heavy ($Ar^+$, $Kr^+$, $Xe^+$) inert gas ions revealed also that the effect of primary radiation damage is less significant than the secondary damage effects because the martensitic transformation induced by

He^{+} ion implantation is effective in the similar way as other heavy inert gas ions. Then, they also [8] detected a small peak of X-ray diffraction patterns from solid phase of Xe[+] in a 17/7 and17/13 stainless steel implanted with $1 \times 10^{21}$ Xe-ions m[-2]. The lattice constant obtained from the broad diffraction peak indicates that the pressure in the inclusions is about 5 GPa. Furthermore, Sakamoto et al [10] found that the solid phase inclusions are formed by agglomeration of the implanted inert gas atoms in type-304 stainless steel. On the other hand, the present results in the next chapter and the previous results [12,7,13] also revealed that the transformed regions decrease to the depth. Nucleation of the

martensitic transformation looks like to start from the surface layer to depth regions and not from the regions have high concentration of implanted ions.

In this work revealed that the orientation relationships is found agree with the orientation relationship of the K-S rules. Although mechanism of the difference of the orientation relationship not well understood but it is probably related with experimental condition such as type and condition of bulk materials, and implanted-ion types. Johnson et al suggested that the observed N-W orientation relationship, it may be associated with the existence of Frank dislocation loops [14] in the implanted samples.
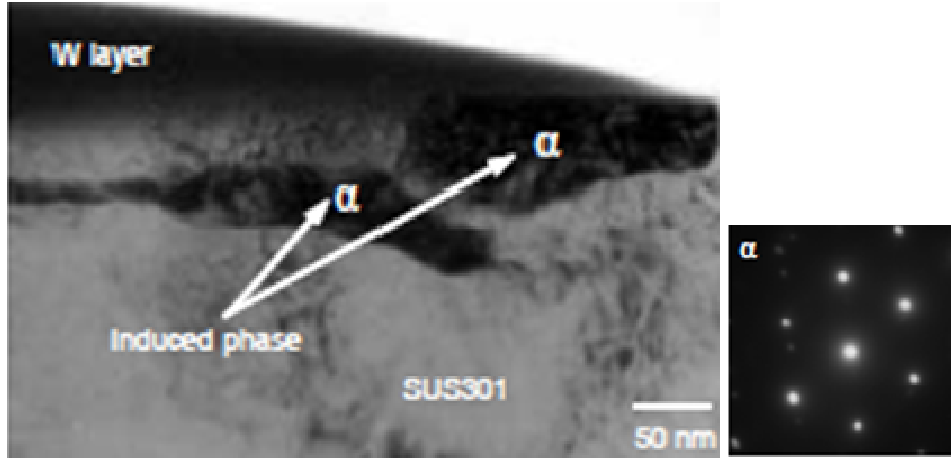


**Figure 3:** (a) TEM bright field image of austenitic stainless steel 301SS implanted with 200 keV Ti^{+} at room temperature to dose of $5 \times 10^{20}$ ions m[-2] and (b) SAD patterns corresponded to implantation induced martensite phase
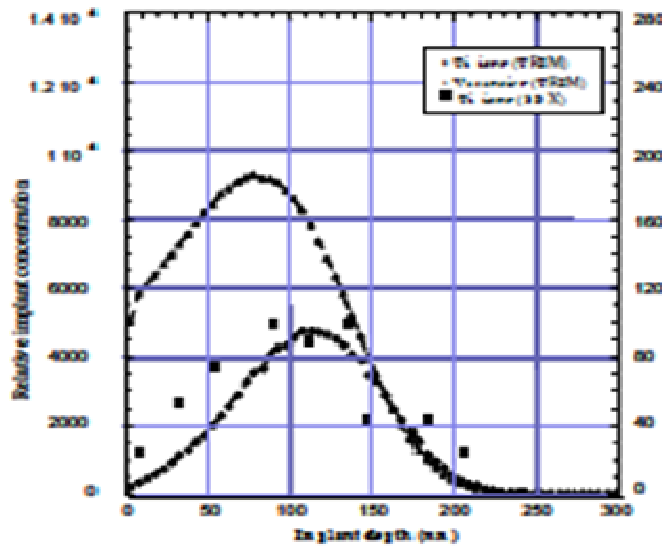


**Figure 4:** Depth distribution profile of ions and vacancies after implantation of 300 keV Ti ions to dose of 5 x 10^{20} ions m[-2] onto austenitic stainless steel measured using EDX analysis (■) and calculated using TRIM code computer program (------)
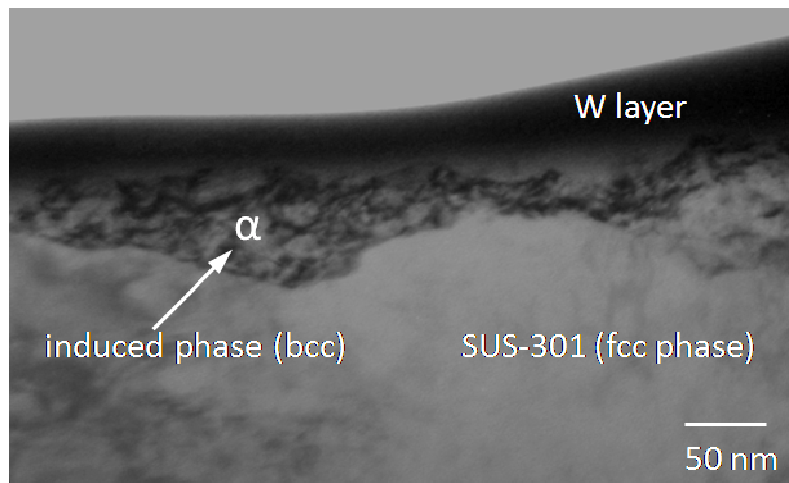
**Figure 5:** TEM bright field image of austenitic stainless steel 301SS implanted with 300 keV Ti$^+$ at room temperature to dose of 5x10$^{20}$ ions m$^{-2}$.

## 4. CONCLUSION

The TEM observations for depth distribution profile of the implanted surface found that the martensite phase is seem to be started for nucleation at surface region away from the peak position of highest implanted ion concentration. The regions have larger ion concentration difference (larger concentration gradient) which may give rising the local stress concentration caused by lattice strain due to embedded ions. Furthermore the increasing the internal stress near the surface introduced by damage due to implantation may induce the transformation.

## ACKNOWLEDGEMENT

## REFERENCES

[1]     E. Johnson, T. Wohlenberg, and W.A. Grant, *Phase Transitions*, 1(1979a) 23.
[2]     E. Johnson, T. Wohlenberg, W.A. Grant, P. Hansen, and L.T.Chadderton, *J. Microscopy*, 116 (1979b) 77.
[3]     E. Johnson, U. Littmark, A. Johansen and C Christodoulides, *Phil. Mag. A*, 45 (1982) 803.
[4]     N. Hayashi and T. Takahashi, *Appl. Phys. Lett*, 41 (1982) 1100.
[5]     N. Hayashi, I. Sakamoto and T. Takahashi, *J. Nucl. Mater*, 128/129 (1984) 756.
[6]     E. Johnson, A. Johansen, L. Sarholt- Kristensen, L. Grabaek, N. Hayashi, and I. Sakamoto, *Nucl. Instr. and Meth*, B19/20(1987) 171.
[7]     I. Sakamoto, N. Hayashi, B. Furubashi, and H. Tanoue, *J. Appl. Phys*, 68 (1990) 4508.
[8]     G. Xie, M. Song, K. Mitsuishi, and K. Furuya, *J. Nucl. Mater*, 281 (2000) 80.
[9]     H.H. Andersen, J. Bohr, A. Johansen, E. Johnson, L. Sarholt-Kristensen and V. Surganov, *Phys. Rev. Lett*, 59(1987) 1589.
[10]    I. Sakamoto, N. Hayashi, B. Furubashi, and H. Tanoue, *Hyperfine Interactions*, 42 (1988) 1005.
[11]    E. Johnson, E. Gerritsen, N.G. Chechenin, A. Johansen, L. Sarholt- Kristensen, H.A.A. Keetels, L. Grabaek, and J. Bohr, *Nucl. Instr. and Meth*, B39(1989) 573.
[12]    A. Johansen, E. Johnson, L. Sarholt- sen, S. Steenstrup, E. Gerritsen, C.J.M. KristenDenissen, H. Keetels, J. Politiek, N. Hayashi, and I. Sakamoto, *Nucl. Instr. and Meth*, B50 (1990) 119.
[13]    N. Hayashi, E. Johnson, A. Johansen, L. Sarholt-Kristensen, and I.Sakamoto, *Proceedings of International Conference on Martensitic Transformation*, Nara (The Japan Institute of Metals, Sendai), (1986) 539.
[14]    T.M. Robinson and M.L. Jenkins, *Phil. Mag*. A43 (1981) 999.